Bent-Core Liquid Crystals from Roof-Shaped Boron Coordination Compounds: Synthesis, Characterization, Dielectric, and Electro-Optic Studies

Emma Cavero,[†] M. Rosario de la Fuente,[‡] Eduardo Beltrán,[†] Pilar Romero,[†] José Luis Serrano,[†] and Raquel Giménez*[,†]

Departamento de Química Orgánica y Química Física, Área de Química Orgánica, Facultad de Ciencias-Instituto de Ciencia de Materiales de Aragón, Universidad de Zaragoza-CSIC, 50009 Zaragoza, Spain, and Departamento de Física Aplicada II, Facultad de Ciencias, Universidad del Pais Vasco, 48080 Bilbao, Spain

Received July 31, 2007. Revised Manuscript Received September 28, 2007. Accepted October 2, 2007

Bent-core liquid crystals derived from boron coordination compounds have been obtained using a novel approach that incorporates a roof-shaped pyrazabole ring at the core, and lateral wings of different lengths in their aromatic and aliphatic parts. The materials were characterized in solution and in the pure state. Mesophase behavior was studied by polarized light microscopy, differential scanning calorimetry, X-ray scattering, and solid-state NMR. All of the compounds display a nematic mesophase that is not typical of standard nematic phases as a consequence of their bent shape and their transverse dipole moment. The nonstandard behavior was investigated by dielectric spectroscopy and electro-optic studies. Additionally, some compounds display a direct transition from the fluid nematic phase to a crystal-like phase with a very well-defined layer structure. Compounds with extended aromatic structures exhibit additional mesophases, and these were characterized as intercalated smectic mesophases (B_6). A novel transition from a tilted B_6 phase to a nontilted B_6 phase is described for one of these extended derivatives.

Introduction

Bent-core liquid crystals constitute a fascinating class of polar soft materials.[1] Their molecular structure, in terms of shape and symmetry, possesses a neat transverse dipole moment that can give rise to arrangements that may show ferroelectric, antiferroelectric, and nonlinear optical properties with achiral molecules.[2–6] Moreover, bent-core mesogens are also candidates to exploit the biaxial nematic phase,[7] a new phase with important technological applications in fast switching displays, which has recently been described and confirmed for the first time in a low-molecular-weight thermotropic liquid crystal with a bent-rod molecule derived from 2,5-oxadiazole.[8,9]

The rich phenomenology and properties observed in these materials have inspired researchers in the synthesis of bent-core materials and driven the search for new structures. The design of bent-core molecules, also named banana-like mesogens, generally consists of organic molecules with a central core disubstituted with two mesogenic or promesogenic rodlike moieties with a central in-plane angle between 109° and 140° (Figure 1a).[6] The cores studied are, among others, meta-substituted phenyl rings (e.g., resorcinol derivatives), a biphenyl or naphthalene substituted at ca. 120°, disubstituted methylene or other flexible spacers with an odd number of atoms, or a heterocycle substituted in 1,3 relative positions (azole rings). Apart from the rodlike substituents, other smaller substituents (CH_3, F, Cl, Br, CN, and NO_2) are often included at any position of the molecule in order to modulate the properties.

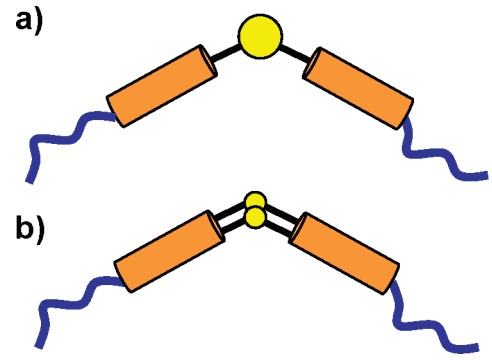

Figure 1. (a) Standard design of bent-core liquid crystals: "in-plane angle". (b) Novel approach followed in this work: "roof-shaped core".

We have recently found that bent-core liquid crystals with a transverse dipole moment can also be obtained by a different molecular design consisting of the introduction of a "two-point bend", instead of the conventional "in-plane

* To whom correspondence should be addressed. Phone: +34-976-762277. Fax: +34-976-762686. E-mail: rgimenez@unizar.es.
[†] Universidad de Zaragoza-CSIC.
[‡] Universidad del Pais Vasco.

(1) Ros, M. B.; Serrano, J. L.; de la Fuente, M. R.; Folcia, C. L. *J. Mater. Chem.* **2005**, *15*, 5093–5098.
(2) Pelzl, G.; Diele, S.; Weissflog, W. *Adv. Mater.* **1999**, *11*, 707–724.
(3) Walba, D. M.; Körblova, E.; Shao, R.; Maclennan, J. E.; Link, D. R.; Glaser, M. A.; Clark, N. A. *Science* **2000**, *288*, 2181–2184.
(4) Tschierske, C.; Dantlgraber, G. *Pramana J. Phys.* **2003**, *61*, 455–481.
(5) Takezoe, H.; Takanishi, Y. *Jpn. J. Appl. Phys. A* **2006**, *45*, 597–625.
(6) Reddy, R. A.; Tschierske, C. *J. Mater. Chem.* **2006**, *16*, 907–961.
(7) Luckhurst, G. R. *Nature* **2004**, *430*, 413–414.
(8) Madsen, L. A.; Dingemans, T. J.; Nakata, M.; Samulski, E. T. *Phys. Rev. Lett.* **2004**, *92*, 145505(4) .
(9) Acharya, B. R.; Primak, A.; Kumar, S. *Phys. Rev. Lett.* **2004**, *92*, 145506(4) .

10.1021/cm702129s CCC: $37.00
Published on Web 11/14/2007

Scheme 1

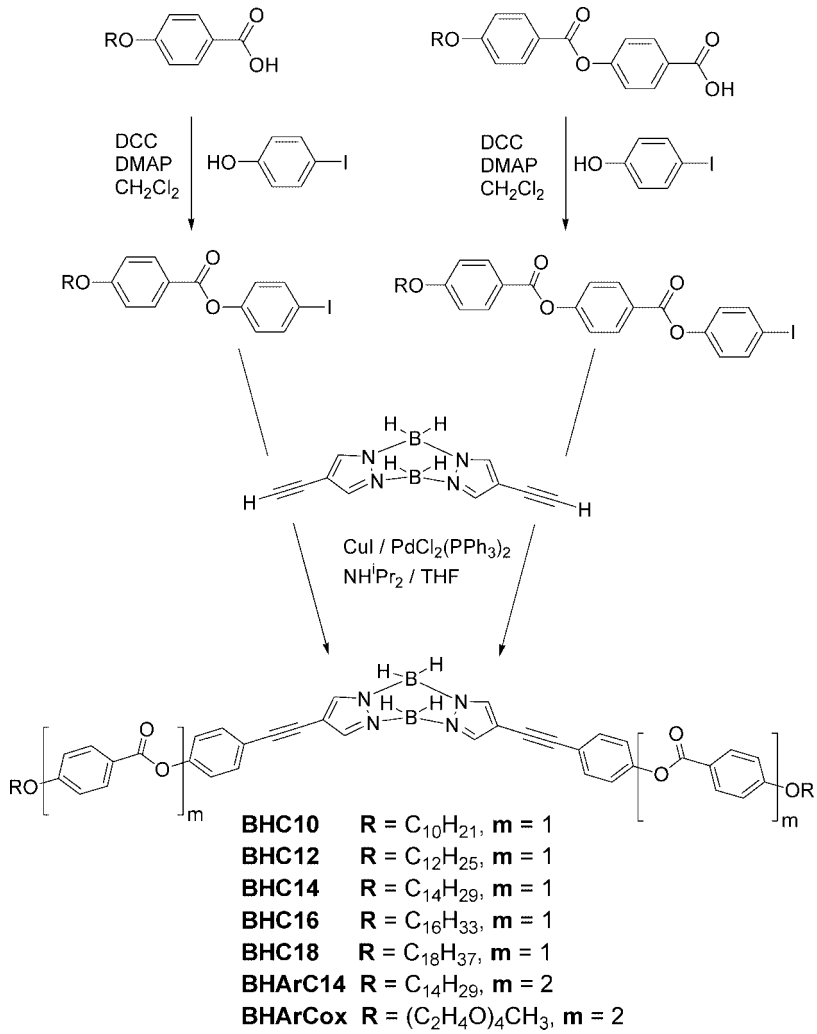

BHC10 R = $C_{10}H_{21}$, **m** = 1
BHC12 R = $C_{12}H_{25}$, **m** = 1
BHC14 R = $C_{14}H_{29}$, **m** = 1
BHC16 R = $C_{16}H_{33}$, **m** = 1
BHC18 R = $C_{18}H_{37}$, **m** = 1
BHArC14 R = $C_{14}H_{29}$, **m** = 2
BHArCox R = $(C_2H_4O)_4CH_3$, **m** = 2

angle", as the origin of the bent shape (Figure 1). This has been achieved by including a roof-shaped pyrazabole ring at the core.[10] The pyrazabole heterocycle is a boron coordination compound derived from pyrazole[11,12] with a roof shape arising from the stable boat conformation of the central B_2N_4 ring. The boat conformation of BH_2-pyrazaboles is C_{2v} symmetric and forms an angle of 130–134°.[13,14] Their structural characteristics make them appropriate candidates to obtain novel bent-core liquid crystals.

Indeed, we have prepared several bent-shaped molecules by substitution of the pyrazabole ring at the 2 and 6 positions with rodlike moieties of different lengths. These rodlike moieties, also called lateral wings, include two aromatic rings and a series of aliphatic chains (**BHCn**, $n = 10$, 12, 14, 16, 18), or three aromatic rings (**BHArC14, BHArCox**) (Scheme 1). In the last example, **BHArCox**, an oxyethylenic terminal chain is introduced in order to decrease the transition temperatures with respect to the aliphatic analogue **BHArC14**. All of these compounds are liquid crystals and display novel lamellar and nematic phases, which were characterized by spectroscopic techniques and X-ray diffraction (XRD). The nematic phase was investigated by dielectric spectroscopy and electro-optic studies displaying a nonstandard behavior under electric fields.

Results and Discussion

Synthesis and Characterization in Solution. The synthesis of the pyrazaboles was carried out by a convergent pathway according to Scheme 1. The compounds were prepared by a double Sonogashira cross-coupling reaction[15] of 2,6-bis(ethynyl)pyrazabole[10] with 2 equiv of the corresponding aryl iodide. The pyrazabole ring is stable under these conditions. The reaction proceeds with moderate yields and proved to be a better option than the coupling of 2,6-diiodopyrazabole with an arylacetylene, as homocoupling products are minimized with the first procedure in a similar way to that of the pyrazole derivatives.[16] The formation of

(10) Cavero, E.; Lydon, D. P.; Uriel, S.; De la Fuente, M. R.; Serrano, J. L.; Giménez, R. *Angew. Chem., Int. Ed.* **2007**, *119*, 5267–5269.
(11) Trofimenko, S. *J. Am. Chem. Soc.* **1966**, *88*, 1842–1844.
(12) Trofimenko, S. *J. Am. Chem. Soc.* **1967**, *89*, 3165–3170.
(13) Cavero, E.; Giménez, R.; Uriel, S.; Beltrán, E.; Serrano, J. L.; Alkorta, I.; Elguero, J. *Cryst. Growth Des.* Submitted.
(14) Barberá, J.; Giménez, R.; Serrano, J. L. *Chem. Mater.* **2000**, *12*, 481–489.
(15) Sonogashira, K. *J. Organomet. Chem.* **2002**, *653*, 46–49.
(16) Vasilevsky, S. F.; Tretyakov, E. V.; Elguero, J. *Adv. Heterocycl. Chem.* **2002**, *82*, 1–99.

Table 1. Mesomorphic Behavior of Pyrazabole Derivatives

compound	cycle	phase transitions T/°C (ΔH/kJ mol^{-1})
BHC10	1st heating	Cr 114 (11.3) Cr′ 158 (54.0) N 169 (2.7) I
	1st cooling	I 168 (2.0) N 135 (53.3) Cr′
BHC12	1st heating	Cr 106 (26.8) Cr′ 135 (58.3) N 153 (2.8) I
	1st cooling	I 152 (2.8) N 117 (52.3) Cr′
BHC14	1st heating	Cr 99 (55.4) B_x 121 (31.9) N 145 (2.5) I
	1st cooling	I 145 (2.5) N 117 (30.0) B_x
BHC16	1st heating	Cr 99 (68.9) B_x 120 (33.4) N 135 (2.1) I
	1st cooling	I 135 (2.7) N 116 (30.0) B_x
BHC18	1st heating	Cr 104 Cr′ 112 (74.6)[a] B_x 120 (33.3) N 130 (1.8) I
	1st cooling	I 129 (1.7) N 116 (34.5) B_x
BHArC14	1st heating	Cr 106 (38.8) B_y 161 (30.3) B_{6tilt} 202 (1.8)[b] B_6 (233 N)[c]
	1st cooling	(N 230)[c] B_6 202 (1.1) B_{6tilt} 150 (24.9) B_y
BHArCox	1st heating	Cr 114 (21.2) B_y 133 (23.8) B_{6tilt} 178 (0.2)[b] N
	1st cooling	N 177 (0.2) B_{6tilt} 131 (22.1) B_y

[a] Enthalpy sum of two transitions. [b] Sample decomposition after the transition. [c] POM data.

the pyrazabole derivatives is evidenced by the infrared spectra. The characteristic ≡C−H stretching band observed in the 2,6-bis(ethynyl)pyrazabole at 3300 cm^{-1} disappears after the cross-coupling reaction, and a strong carbonyl band is observed at 1730 cm^{-1}. The B−H stretching bands of the pyrazabole ring are observed in the 2460–2415 cm^{-1} region. The ^{1}H NMR and ^{13}C NMR spectra recorded in $CDCl_3$ also provide evidence for the satisfactory coupling. In the ^{1}H NMR spectrum, the ≡C−H proton signal, which appeared as a singlet at 3.5 ppm in the starting material, was not observed for the product, and the C≡C carbon signals were shifted to a lower field in the ^{13}C NMR spectra.

Thermal Behavior. The mesomorphic properties of the pyrazabole derivatives were determined by polarizing optical microscopy (POM) and differential scanning calorimetry (DSC). Transition temperatures and enthalpy values for the first heating and cooling cycles recorded at a rate of 10 °C/min are shown in Table 1. All compounds were obtained as colorless crystalline solids after recrystallization from acetone, dichloromethane, or dichloromethane/hexane (see the Experimental Section) and display a varied polymorphism. In general, the as-obtained crystal phase is not recovered after the first heating cycle.

All of the **BHCn** pyrazaboles (n = 10, 12, 14, 16, and 18) show a nematic mesophase. The clearing point decreases on increasing the chain length. Upon observation by POM, the nematic phase showed threadlike and marbled textures and intense Brownian motion, corresponding to an apparently conventional nematic mesophase. *Schlieren* textures were hardly observed, appearing in the isotropic liquid−nematic transition. In some preparations, domains of opposite-handedness separated by walls were observed by slightly decrossing the polarizers on the optical microscope, in a similar way to those found for other nematic bent-core liquid crystals described previously.[17–20] XRD studies in the

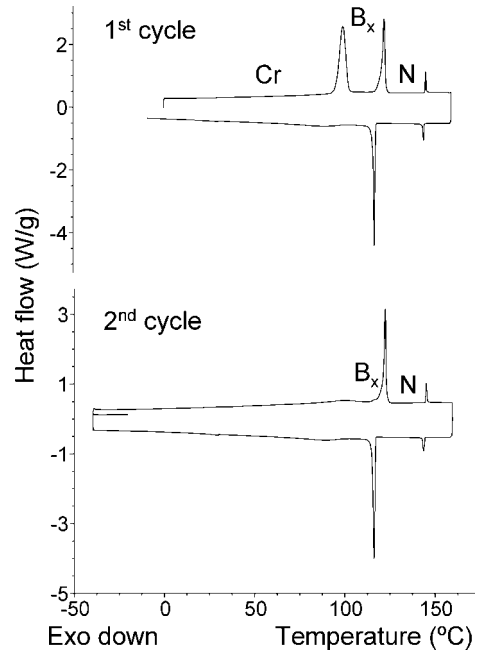

Figure 2. DSC thermogram for **BHC14**.

nematic phase were carried out. Taking into account the similar behavior of the **BHCn** pyrazaboles with different terminal chains, the following XRD discussion refers only to **BHC14**, which showed the widest temperature ranges in their mesophases. The XRD pattern of the nematic phase consisted of a diffuse meridian-reinforced reflection in the small-angle region and a diffuse wide-angle scattering located around the equator.[10] Furthermore, the maximum in the small-angle region was also split. This observation could be due to the presence of smectic C clusters[19] (cybotactic domains) in the uniaxial nematic phase, but this splitting of the small-angle reflections into two pairs has also been associated with the biaxial character of the nematic phase.[9,21] Therefore, these materials are candidates to exhibit biaxial nematic phases.

In addition, the compounds with aliphatic chains longer than 14 carbon atoms (**BHC14**, **BHC16**, and **BHC18**) display, on cooling the nematic phase, a viscous phase at lower temperatures, and this is denoted as B_x (Figure 2). This phase shows very low birefringence and generally appears from the nematic phase as a spherulitic texture with large extinction "Maltese crosses" (Figure 3a). To the naked eye, the B_x phase is transparent and a blue−purple iridiscence can be detected in some cases, depending on the thermal history and the viewing angle. No further changes in the texture are observed on cooling down to room temperature, indicating that the phase remains or freezes at room temperature.

The XRD patterns obtained for the B_x phase presented a set of sharp maxima in the small-angle region of up to sixth order situated at regular spacings, supplying the lamellar layer spacing and indicating a very good layer definition. In the wide-angle region, two reflections are observed, indicating

(17) Pelzl, G.; Eremin, A.; Diele, S.; Kresse, H.; Weissflog, W. *J. Mater. Chem.* **2002**, *12*, 2591–2593.
(18) Schröder, M. W.; Diele, S.; Pelzl, G.; Dunemann, U.; Kresse, H.; Weissflog, W. *J. Mater. Chem.* **2003**, *13*, 1877–1882.
(19) Weissflog, W.; Sokolowski, S.; Dehne, H.; Das, B.; Grande, S.; Schröder, M. W.; Eremin, A.; Diele, S.; Pelzl, G.; Kresse, H. *Liq. Cryst.* **2004**, *31*, 923–933.
(20) Görtz, V.; Goodby, J. W. *Chem. Commun.* **2005**, *3262*, 3264.
(21) Prasad, V.; Kang, S.-W.; Suresh, K. A.; Joshi, L.; Wang, Q.; Kumar, S. *J. Am. Chem. Soc.* **2005**, *127*, 17224–17227.

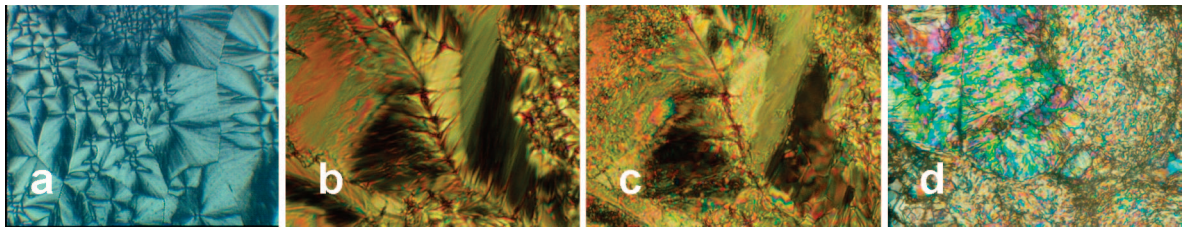

Figure 3. Microphotographs of the (a) B_x phase, (b) B_6 phase, (c) B_{6tilt} phase, and (d) B_y phase.

a crystal-like structure. We did not observe any orientation in the XRD patterns, even when the sample was cooled from partially oriented nematic phases. The XRD patterns of the B_x phase appear similar to those described for the B_4 phase of some bent-core liquid crystals.[22] It is interesting to remember at this point that the B_4 phase has been postulated to be a nontilted lamellar crystal-like phase, as the measured layer spacing is similar to the molecular length. However, in our case, the layer spacing obtained by applying Bragg's law is 52.7 Å at 110 °C, whereas the estimated molecular length, calculated with molecular models and considering a molecular bend angle of 135°, is 71 Å. Hence, the layer spacing in the B_x phase is considerably lower than the estimated molecular length. When the sample was allowed to cool down to room temperature, the same XRD pattern was observed with a slight increase in the layer spacing (53.6 Å), indicating that the structure may have more extended alkyl chains.

To account for the difference between the measured layer spacing and the estimated molecular length, the molecular organization could be consistent with two structural models. On the one hand, a model can be proposed in which the molecules arrange in layers in an orthogonal way such that the difference between the molecular length and the layer spacing arises from the existence of significant interdigitation of the terminal chains (Figure 4a). On the other hand, the decrease in the layer spacing in comparison to the estimated molecular length could result from tilting of the molecules with respect to the layer normal (Figure 4b) by up to 40° in an alternating way (anticlinic model), a situation that would also be in agreement with the low birefringence observed. The formation of smectic C-like clusters in the nematic phase would support the tilted model.

Pyrazaboles with extended aromatic cores (**BHArC14** and **BHArCox**) also display a nematic mesophase, but at higher temperatures than the shorter **BHCn** pyrazaboles. In general, both compounds have limited thermal stability at high temperatures. The transition to the nematic phase is accompanied by gradual decomposition of the sample, which by POM appears as a "boiling" of the *schlieren* texture. If the heating is prolonged further, until the complete disappearance of the nematic texture is reached, a transition is not observed on cooling. Difficulties were also encountered in reproducing temperature transitions in successive DSC cycles once the transition to the nematic phase had been reached.

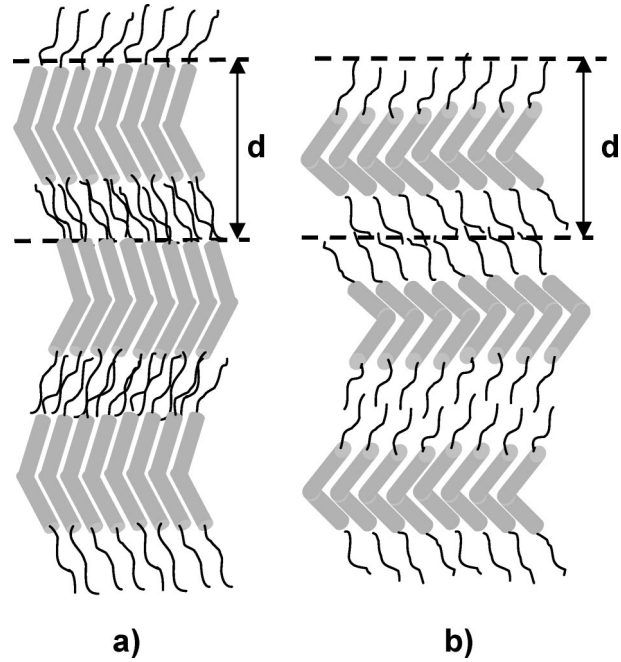

Figure 4. Proposed layer structures in the B_x phase. (a) Interdigitated orthogonal model. (b) Tilted model.

The features shown by **BHArC14** upon examination by POM are described below. Upon heating the solid, a transition was observed at 161 °C to a fluid phase with a grainy texture. At 202 °C, another change was observed to a texture with sharper lines, and this was also detected by DSC as a small peak with an enthalpy of 1.8 kJ mol^{-1}. Further heating leads at 233–240 °C to a gradual change to the *schlieren* and marbled textures of a nematic mesophase, and this is accompanied by decomposition of the sample.

The nonoriented XRD patterns obtained on heating at 170 and at 206 °C show only one sharp reflection in the small-angle region and a broad diffuse reflection in the wide-angle region. The measured layer spacings at both temperatures are 36.1 and 39.9 Å, respectively. Comparison with the molecular data (L = 83 Å assuming a bend angle of 135° and using molecular models) leads one to consider intercalated lamellar structures for these mesophases. The layer spacing of the low-temperature mesophase is shorter than the corresponding estimated half-molecular length, and the spacing for the high-temperature mesophase is about half the molecular length. On the basis of both textural features and XRD data,[2,23] these mesophases have been identified as B_6 mesophases. In the low-temperature phase, the molecules

(22) Thisayukta, J.; Takezoe, H.; Watanabe, J. *Jpn. J. Appl. Phys. A* **2001**, *40*, 3277–3287.

(23) Weissflog, W.; Wirth, I.; Diele, S.; Pelzl, G.; Schmalfuss, H.; Schoss, T.; Würflinger, A. *Liq. Cryst.* **2001**, *28*, 1603–1609.

are tilted with respect to the layer normal (B_{6tilt}),[19] and in the high-temperature phase, the molecules are not tilted (B_6).

When the sample was cooled immediately after the $B_{6tilt}-B_6$ transition, quite reproducible thermal cycles were obtained, and on cooling, the B_6-B_{6tilt} transition was observed as a change in the fan-shaped texture, which became more diffuse at 202 °C (Figure 3b,c). In some cases, four-brush *schlieren*-like textures were also observed. Only a few reports on $N-B_6$ transitions have been described in the literature, and these examples display similar textures and parameters.[19,24] However, this is the first example of a compound with a transition between two B_6 mesophases.

Upon cooling the B_{6tilt} mesophase, a highly birefringent striated texture (Figure 3d) was observed due to a viscous phase that has been assigned as B_y, as this phase has different characteristics in terms of texture and XRD pattern than the B_x phase observed for the **BHCn** derivatives. The phase is not transparent but opaque, and the XRD pattern shows partial orientation. The XRD diffractogram displays a series of reflections in the small-angle region, situated at regular spacings, from which a layer spacing of $d = 59$ Å is calculated. This is consistent with a tilted structure. In the wide-angle region, several reflections are found, indicating the existence of positional order.

The oxyethylenic compound **BHArCox** exhibits lower transition temperatures than the **BHArC14** homologue, and the mesophases are destabilized, as one would expect given that the effect of the oxyethylenic chain is usually to decrease the transition temperatures.[25,26] The compound exhibits a fluid mesophase at 130 °C with grainy and fan-shaped textures, and this transforms into a very fluid threadlike texture of a nematic mesophase at 178 °C. The transition is also observed in the DSC thermogram with a measured enthalpy of 0.2 kJ mol^{-1}. Partial decomposition occurs at this point as an increase in the fluidity is observed along with spasmodic movements and low reproducibility of the subsequent cycles. The XRD pattern at 165 °C showed a single reflection in the low-angle region and a diffuse halo in the large-angle region. The layer spacing of the mesophase is 32.9 Å, which is shorter than the corresponding half-molecular length (78 Å considering a bend angle of 135° and using molecular models). Thus, taking into account the textures and the patterns, a B_{6tilt} phase is proposed. In the cooling cycle, the B_{6tilt} phase transforms into a viscous birefringent phase with similar characteristics to those found for the B_y phase of **BHArC14**, and this remains at room temperature.

^{13}C CP/MAS NMR Spectroscopy. Solid-state NMR measurements were performed in the crystal, B_x, and nematic phases of compound **BHC14** in order to compare the spectra with those previously reported for bent-core liquid crystals with nontilted B_4 and tilted B_2 mesophases.[27–29] The atomic numbering used for the carbon signals is shown in Figure 5 along with the spectra in the first heating and first cooling processes in the temperature range allowed by our instrument setup.

At room temperature, in the virgin crystalline phase (Figure 5a), most of the signals appear as doublets. This pattern is clearly observed for the carbons near the central core (C2, C3, C4, and C5), and it is also observable for the aromatic (C9) and for the first and last carbons of the aliphatic chains (C15 and C18). At 111 °C, in the B_x phase (Figure 5b), most of the doublets converge into a single signal and the aromatic part simplifies, but some characteristics of the previous phase are still retained as C3, and C9 appear as doublets. The carbonyl group, which was overlapped with the C14 signal in the crystal phase at 162.4 ppm, is shifted downfield to 164 ppm in the B_x phase, indicating a possible change in the torsion angle between the carbonyl carbon and the aromatic rings. On the other side, there is a shift of the methylene carbons (ca. 24 ppm) to higher fields owing to a lower proportion of trans conformations in the terminal chains.[30] In the nematic phase, at 140 °C (Figure 5c), a similar spectrum is obtained in which most of the signals appear as broad singlets, which is consistent with a solution ^{13}C NMR spectrum (Figure 5f) and is a consequence of an averaged electronic field around the carbons due to the fluidity of the phase. The spectrum obtained in the nematic phase does not change considerably on cooling to the B_x phase (Figure 5d), indicating that the B_x phase could have some fluid characteristics. In addition, the appearance is more similar to the spectrum reported for B_2 than that for B_4 mesophases,[29] which would be in accordance with the proposal of a smectic tilted model similar to a B_2 phase for the B_x phase. The spectrum hardly changes during the cooling process, indicating that the structure of the B_x phase is preserved at room temperature and the starting crystalline phase is not recovered (Figure 5e).

In the literature, it has been reported that in the B_4 phase of some bent-core liquid crystals the carbonyl signal appears to be split, and this has been related to the fact that both chemically equivalent carbonyl groups adopt different torsion angles.[28] Such a situation reduces the molecular symmetry and gives rise to a conformational molecular chirality, which has been invoked as the origin of the chirality for the B_4 phase. On the other hand, studies performed on the lamellar tilted B_2 phase yielded a different pattern for the carbonyl signal, which in this case is not split but appears as a single broad signal.[29] In the B_x phase of **BHC14**, the carbonyl signal is partially overlapped with the aromatic C14 signal, and this precludes a clear observation of any splitting.

Dielectric Spectroscopy. Dielectric spectroscopy is a powerful tool to study the dynamics of polar substances such

(24) Reddy, R. A.; Sadashiva, B. K. *J. Mater. Chem.* **2004**, *14*, 1936–1947.
(25) Kaminska, A.; Mieczkowski, J.; Pociecha, D.; Szydlowska, J.; Gorecka, E. *J. Mater. Chem.* **2003**, *13*, 475–478.
(26) Barberá, J.; De Francisco, I.; Forcén, P.; Gimeno, N.; Monreal, L.; Ros, B.; Serrano, J. L. In *9th International Ferroelectric Liquid Crystal Conference Dublin*, Trinity College, Dublin, Ireland, Aug 24−29, 2003; p 87.
(27) Sekine, T.; Niori, T.; Sone, M.; Watanabe, J.; Choi, S.-W.; Takanishi, Y.; Takezoe, H. *Jpn. J. Appl. Phys. A* **1997**, *36*, 6455–6463.
(28) Kurosu, H.; Kawasaki, M.; Hirose, M.; Yamada, M.; Kang, S.; Thisayukta, J.; Sone, M.; Takezoe, H.; Watanabe, J. *J. Phys. Chem. A* **2004**, *108*, 4674–4678.
(29) Walba, D. M.; Eshdat, L.; Körblova, E.; Shoemaker, R. K. *Cryst. Growth Des.* **2005**, *5*, 2091–2099.
(30) Ishikawa, K.; Kurosu, H.; Ando, I. *J. Mol. Struct.* **1990**, *248*, 361.

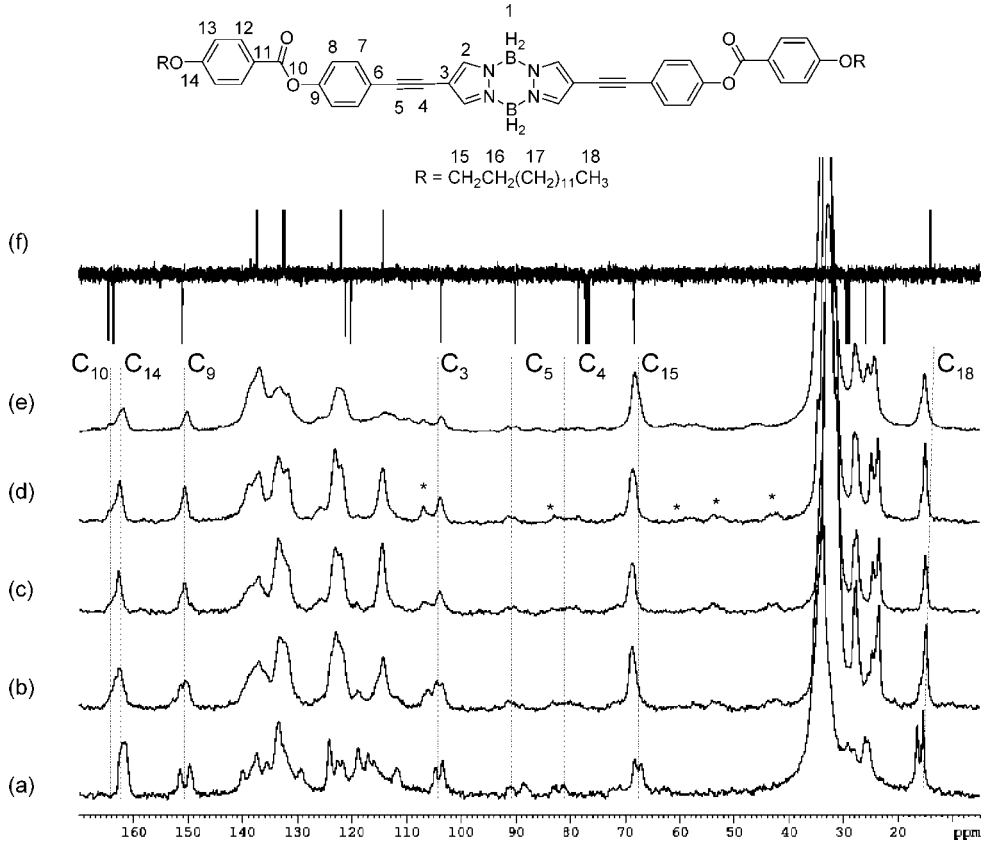

Figure 5. ^{13}C NMR for compound **BHC14**. (a) CP/MAS of the crystal at RT; (b) CP/MAS of the B_x phase at 111 °C; (c) CP/MAS of the N phase at 140 °C; (d) CP/MAS of the B_x phase at 111 °C (on cooling from the N phase); (e) CP/MAS of the B_x phase at RT (on cooling from the N phase); (f) APT in solution ($CDCl_3$). *ssb of rotation. (The spinning rate for spectra b−e was 8 kHz and for a was 10 kHz.)

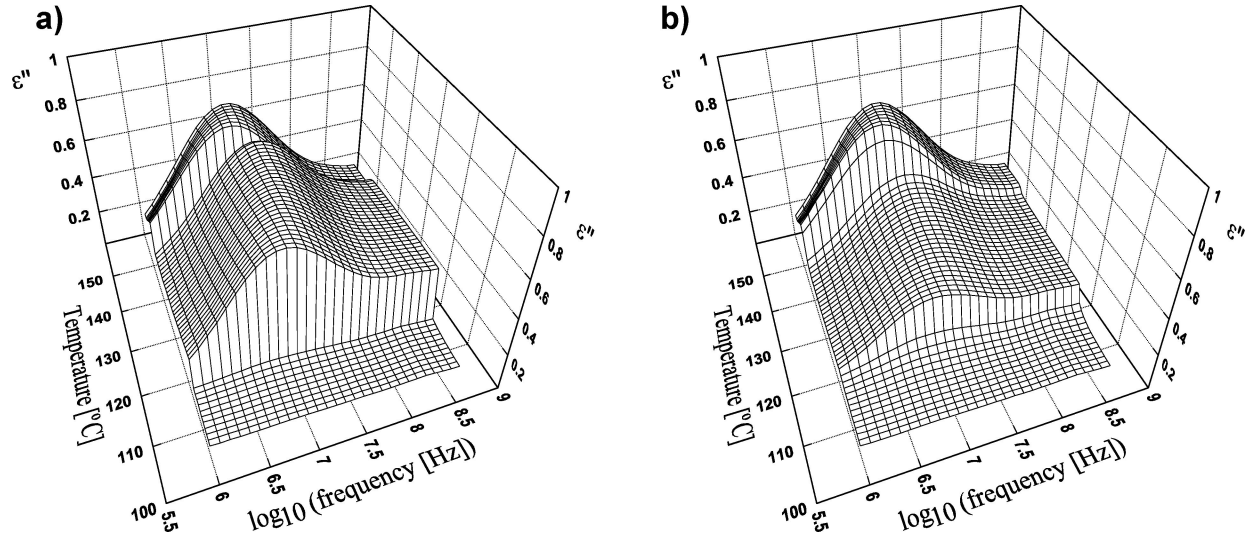

Figure 6. Three-dimensional plot of the dielectric losses vs temperature and frequency, metallic cell, 50-μm-thick. (a) 0 V bias voltage; (b) 40 V bias voltage.

as liquid crystals. This technique provides information about dipoles and molecular dynamics. Analysis of the complex dielectric permittivity as a function of frequency and temperature provides information about the molecular motions that involves changes in the dipole moments. The behavior of the nematic phase in the shorter analogs was studied, and the results for compound **BHC14** are shown as a representative example. In nematic phases, the molecular motions mainly involve rotation around the molecular long axis, which is associated with the transverse dipole moment, rotation around the molecular short axis, which involves the longitudinal dipole, and the precession of the long axis around the director, which also involves the longitudinal dipole.[31] A three-dimensional plot of the losses versus the temperature and frequency for compound **BHC14** is shown in Figure 6 (only the 10^6 to 10^9 Hz frequency range is represented because, excluding the dc conductivity contribution, the dielectric response is almost flat for lower frequencies).

(31) Diez, S.; Perez-Jubindo, M. A.; De la Fuente, M. R.; López, D. A.; Salud, J.; Tamarit, J. L. *Liq. Cryst.* **2006**, *33*, 1083–1091.

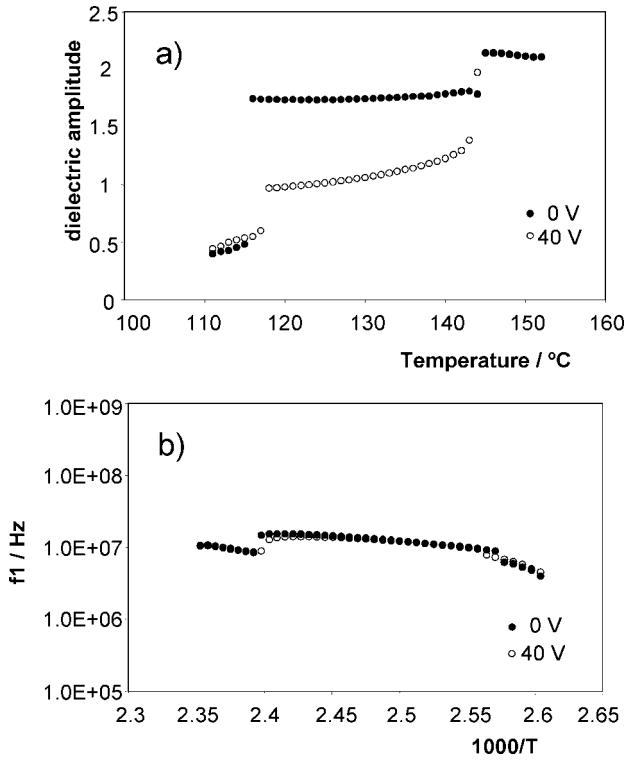

Figure 7. (a) Dielectric amplitude of mode 1, rotation around the molecular long axis, vs temperature. (b) Relaxation frequency of mode 1, rotation around the molecular long axis, vs the reciprocal temperature.

The spectrum is dominated by a mode with a frequency of around 10^7 Hz in both the nematic and isotropic phases. However, a smaller, but noticeable, relaxation at high frequency (near 10^9 Hz) is also present. In order to determine amplitudes, frequencies, and activation energies for each process, the experimental data for each phase were fitted to eq 1

$$\varepsilon(\omega) = \sum_k \frac{\Delta\varepsilon_k}{[1 + (i\omega\tau_k)^{\alpha_k}]^{\beta_k}} + \varepsilon_\infty \qquad (1)$$

where $\Delta\varepsilon_k$ accounts for the dielectric amplitude of each mode and ε_∞ the high-frequency permittivity. In our case, $k = 2$ and both modes follow the Cole–Cole function: $\beta_k = 1$ and $\alpha_1 = 0.8$ for the low-frequency mode (mode 1) and $\alpha_2 = 0.75$ for the high-frequency one (mode 2). $f_k = 1/2\pi\tau_k$ is the relaxation frequency of each mode. Both components of the complex dielectric permittivity were fitted simultaneously. A plot of the dielectric amplitude of mode 1 (we believe that mode 2 should be related to some intramolecular contribution) versus the temperature is shown in Figure 7a, and an Arrhenius plot of its characteristic frequency versus the temperature is shown in Figure 7b. Within each phase, f_1 follows the Arrhenius law with an activation energy of 55 kJ mol^{-1} in the isotropic phase and 28 kJ mol^{-1} in the nematic phase. At the I−N phase transition, this parameter increases. This temperature behavior is typical of rotations around the molecular long axis. The nematic potential accelerates this motion, allowing an increase in the characteristic frequency at the onset of nematic order. Moreover, additional relaxation was not observed at lower frequencies, and this can be attributed to rotation around the short axis, which would indicate that these molecules have only a net transverse dipole moment, as expected from their bent symmetrical shape. It is also important to note that the characteristic frequencies in the isotropic phase are between one and two decades smaller than for conventional rodlike nematics[31] and on the order of those obtained for bent-shaped compounds.[32,33]

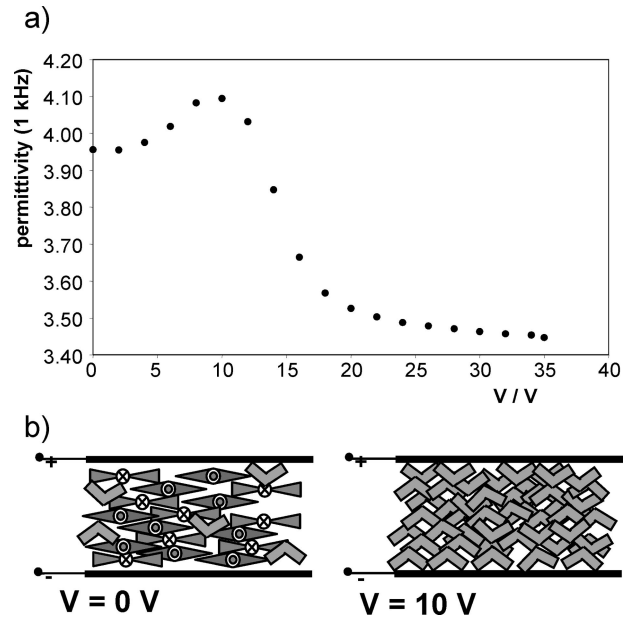

Figure 8. (a) Dielectric permittivity vs bias voltage, 5-μm-thick Linkam cell. (b) Schematic illustration of the molecules in a planar cell.

Before considering the dielectric amplitudes, the results obtained under a dc voltage of 40 V will be discussed (Figure 6b). This spectrum is very similar to that obtained without any dc voltage (amplitudes and frequencies are also represented in Figure 7a,b). At 0 V, the dielectric amplitude decreases at the I−N phase transition. When an almost planar alignment is assumed (checked by comparison with the static permittivity obtained in a planar transparent cell), this decrease is only possible if there is a strong antiparallel correlation of transverse dipole moments. The strength at 40 V is smaller than that found at 0 V. With the application of a dc field to a compound with negative dielectric anisotropy (as should be the case here because the molecules only have a transverse dipole moment), the short axes tend to align along the field, and as a result, the corresponding dielectric amplitude, related to the transverse dipole, should increase. However, in our case, this parameter decreases. In an effort to analyze this effect in more detail, we measured the dielectric permittivity at 1 kHz (a frequency low enough to be considered as a static permittivity) as a function of the applied voltage in a Linkam planar cell (5 μm thick), in which the material was perfectly aligned in the N phase (Figure 8a). Initially, up to 10 V, the permittivity increases, and then at higher voltages, it decreases. One has to take into account that these molecules are not rodlike but biaxial and therefore have two different short axes. The effect of

(32) Diez, S.; De la Fuente, M. R.; Jubindo, M. A. P.; Ros, B. *Liq. Cryst.* **2003**, *30*, 1407–1412.
(33) Ortega, J.; de la Fuente, M. R.; Etxebarria, J.; Folcia, C. L.; Diez, S.; Gallastegui, J. A.; Gimeno, N.; Ros, M. B.; Perez-Jubindo, M. A. *Phys. Rev. E: Stat., Nonlinear, Soft Matter Phys.* **2004**, *69*, 011703.

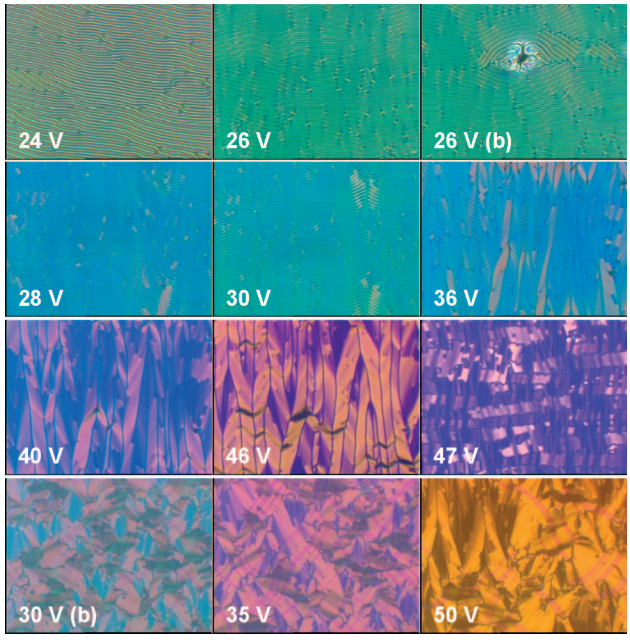

Figure 9. POM microphotographs of the interference patterns registered at different voltages. Picture sizes are 220-μm-long. The polarizer and analyzer are situated in the vertical and horizontal axes, respectively. The nematic director was originally in the horizontal axis.

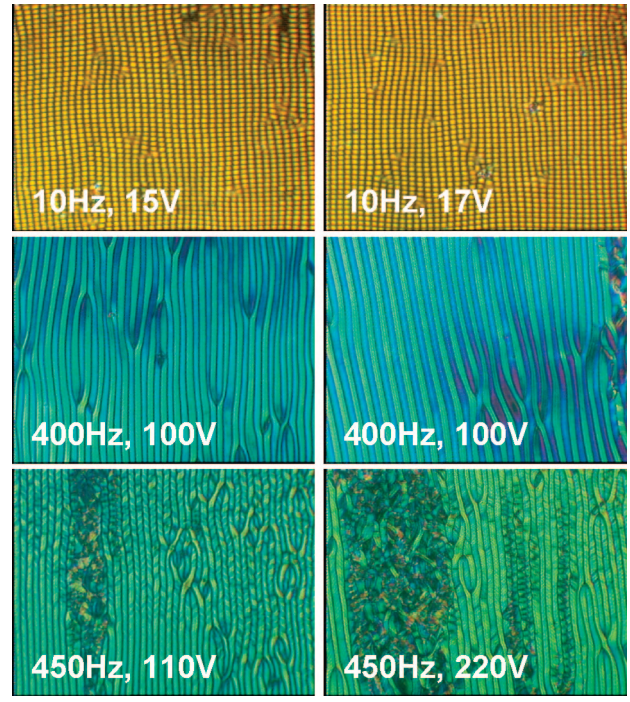

Figure 10. POM microphotographs of the interference patterns obtained by applying alternating voltages (harmonic or triangular).

the field could be to align the short axis with longer polarizability, that is, the axis coinciding with the dipole moment, in the field direction (Figure 8b). For voltages higher than 10 V, the permittivity decreases. This value is also associated with the appearance of electrohydrodynamic interference patterns (see below). When this happens, a proportion of the molecules do not have their long axis parallel to the electrode surface but arbitrary angles are formed, which makes the permittivity decrease. A similar effect was also observed in other compounds.[34] The results for the B_x phase were also plotted, but in this case, the confidence level is lower because the strength decreases markedly. Nevertheless, a clear decrease of the permittivity is observed with an increase in the activation energy, a situation typical of in-plane ordered mesophases.

Electro-Optic Studies. Compound **BHC14** shows interesting properties in the nematic phase upon analyzing the texture changes under different electric fields. This compound exhibits similar properties to other bent-shaped molecules that have recently been reported.[6,18,19,35,36] Upon applying a dc field to a nematic phase oriented in a planar manner (Linkam cell, 5-μm-thick), a domain pattern with equidistant stripes parallel to the original director orientation is observed for voltages up to around 30 V (Figure 9). The distance between lines decreases as the voltage increases, and sometimes the lines are disturbed in defects caused by turbulence (see 26 V (b) in Figure 9). Upon increasing the voltage further (36, 40, and 46 V), a different pattern develops, with leaves appearing perpendicular to the original orientation of the director that are reminiscent of the "banana leaves" of the columnar B_1 phase.[33] At 47 V, the appearance changes once more; it is similar to one reported in the literature[6,18] for a bent-core compound, denoted as N_x, and manifests itself as the presence of short-range positional order with cybotactic domains. In some instances, fan-shaped textures were observed that are similar to those seen for smectic and cholesteric phases (see 30 V (b), 35 V, and 50 V in Figure 9), which have also been observed by other authors.[19,35] This field-induced transition from a planar into a fanlike texture was tentatively attributed[19] to a structure that was originally partially twisted. This could also be the case here, bearing in mind the formation of chiral domains previously described.[10]

When applying harmonic voltages (Figure 10), the electroconvection patterns changed. At low frequencies, the stripes are parallel to the original direction of the director, as with dc voltages. Under certain conditions, for example, 10 Hz and 15 V and 10 Hz and 17 V, the pattern is bidimensional and very regular. Upon increasing the frequency, it is necessary to increase the voltage to obtain the same pattern. Upon increasing the frequency further, this type of pattern disappears and the lines run perpendicular to the original orientation of the director, with some dislocations (see Figure 10, 400 Hz, 100 V). This pattern has been described for other bent-shaped compounds, and these were called "prewavy instabilities";[36] the bright broad stripes are due to periodic director modulations in the glass plane, where the dark narrow lines are the regions in which the director is perpendicular. The wavelength of this modulation is slightly smaller than the thickness of the cells (around 4.5 μm). Upon further increasing the voltage, the disclinations evolve into "wavy patterns" (450 Hz and 110 V and 450 Hz and 220

(34) Diez, S.; Dunmur, D. A.; De la Fuente, M. R.; Karahaliou, P.; Mehl, G. H.; Meyer, T. A. P.-J. M.; Photinos, D. *Liq. Cryst.* **2003**, *30*, 1021–1030.
(35) Kovalenko, L.; Schröder, M. W.; Reddy, R. A.; Diele, S.; Pelzl, G.; Weissflog, W. *Liq. Cryst.* **2005**, *32*, 857–865.
(36) Wiant, D.; Gleeson, J. T.; Éber, N.; Fodor-Csorba, K.; Jákli, A.; Tóth-Katona, T. *Phys. Rev. E: Stat., Nonlinear, Soft Matter Phys.* **2005**, *72*, 041712(12) .

V). Although numerous authors have observed similar phenomena in different compounds,[6,18,19,35,36] the explanation for these electro-hydrodynamic instabilities is not clear. As pointed out by Wiant et al.[36] for the low-frequency behavior, both the standard model including the flexoelectric effect and also an isotropic mechanism could drive the instabilities. An isotropic mechanism is also proposed for the "prewavy instabilities".

Summary and Conclusions

New bent-core liquid crystals have been prepared by coupling two rodlike substituents to the roof-shaped pyrazabole ring using a Sonogashira cross-coupling reaction. The compounds possess a transverse dipole moment and negative dielectric anisotropy. It was found that a low-viscosity, easy-to-orient nematic mesophase is obtained for the shorter pyrazaboles **BHCn**. The nematic phase displays unusual behavior under electric fields, and this is related to the bent molecular shape and could be flexoelectric in origin. Increases in the length of the aliphatic terminal chains gave rise to the appearance of a new crystal-like phase with low birefringence and a very well-defined lamellar structure below the nematic phase, for which a tilted lamellar structure is proposed. Pyrazaboles with extended aromatic cores, **BHArC14** and **BHArCox**, give rise to intercalated lamellar mesophases of the B_6 type in addition to nematic mesophases, with the description for the first time of a transition from a tilted B_6 to a nontilted B_6 phase. The oxyethylenic terminal chain lowers the transition temperatures in comparison to the tetradecyloxy chain but displays poorer thermal stability. The bend angles in these molecules are in the upper range reported for bent-core liquid crystals, which may promote the formation of nematic phases, as observed with 2,5-oxadiazole derivatives[37] and other halogen-substituted resorcinol derivatives.[19] An increase in the size of the aromatic part leads to a partial microsegregation between the aromatic rings and the aliphatic chains, as intercalated layered mesophases are obtained. This effect is not sufficient to generate monolayers in the fluid state. However, very well-defined layered structures are formed in the crystal-like phases of the low-temperature phases formed on cooling the nematic or the B_6 mesophases.

The fact that these compounds tend to interdigitate in an antiparallel way could make them of interest as dopants to stabilize antiferroelectric phases. Moreover, the compounds readily give rise to spontaneous or field-induced twisting that may be frozen in the low-temperature phase. This area will be the subject of future research.

Experimental Section

General Methods. The synthesis of the final pyrazabole derivatives was achieved by a Sonogashira coupling[15] between 2,6-bis(ethynyl)pyrazabole[10] and aryl iodides. A general procedure is included below. The alkoxy-substituted iodide derivatives were prepared by esterification of the corresponding benzoic acids and commercially available iodophenol according to literature methods.[38] The characterization of these compounds will be reported elsewhere. ^{1}H and ^{13}C NMR spectra were recorded on a Bruker AVANCE-400 spectrometer. CP/MAS spectra were recorded on a Bruker AVANCE-400 spectrometer using a 4 mm narrow-bore probe at a spinning rate of 8 kHz; proton decoupling was carried out using TTPM modulation. Infrared spectra were obtained with Nicolet Avatar 380 FTIR (using KBr pellets) and Perkin-Elmer 1600 (using Nujol, NaCl) spectrophotometers. Elemental analyses were performed with a Perkin-Elmer 2400 analyzer. Mass spectra were obtained with a VG Autospec EBE with FAB-LSIMS using nitrobenzyl alcohol as the matrix or a Microflex-Bruker apparatus by MALDI using dithranol as the matrix. Mesomorphic behavior and transition temperatures were examined using an Olympus BH-2 polarizing microscope equipped with a Linkam THMS 600 hot-stage central processor and a CS196 cooling system. DSC was carried out using a DSC 2910 and a Q-1000 from TA Instruments, with samples sealed in aluminum pans and with a scanning rate of 10 °C/min under a nitrogen atmosphere. Both instruments were calibrated with indium (156.6 °C, 28.44 J/g) as the standard. Powder X-ray diffraction patterns were obtained using a Pinhole camera (Anton-Paar) using Ni-filtered Cu Kα radiation. The samples were held in Lindemann glass capillaries ($\Phi = 1$ mm) and heated with a variable temperature attachment. The diffraction patterns were collected on flat photographic film. Dielectric measurements were performed in the range 10^2 to 1.8×10^9 Hz using HP4192A and the Agilent 4291A impedance anlyzers. The cell consisted of two gold-plated electrodes of 5 mm diameter separated by 50-μm-thick silica spacers, making a parallel plate capacitor located at the end of a coaxial line. A modified HP16091A coaxial test fixture was used as the sample holder. The sample was held in a cryostat from Novocontrol, which screens the system, and both temperature and dielectric measurements were computer-controlled.

General Procedure for the Preparation of the Liquid Crystalline Pyrazaboles. A Schlenk tube containing 1 mmol of the corresponding 4-iodophenyl-4′-alkoxybenzoate or 4-iodophenyl-4′-(4"-alkoxybenzoyloxy)benzoate, 0.01 mmol of dichlorobis(triphenylphosphine)palladium(II), 0.02 mmol of copper(I) iodide, and 15 mL of dry THF was degassed on a vacuum line by repeatedly alternating between an argon atmosphere and a vacuum. A total of 1.6 mmol of diisopropylamine was then added. Finally, a solution of 0.55 mmol of the 2,6-bis(ethynyl)pyrazabole in THF (3 mL) was added dropwise, and the reaction mixture was stirred at 55 °C for 24 h. The reaction mixture was then filtered through a pad of Celite and the solution evaporated to dryness. The crude product was purified by column chromatography on silica gel (35–70 μm) using the appropriate eluent as a first step and by recrystallization as a second step.

BHC10. *2,6-bis(4″-Decyloxybenzoyloxypheny1–1′-yl-ethynyl)-pyrazabole*. Eluent: 1:1 dichloromethane/hexane. Recrystallization: acetone. ^{1}H NMR (400 MHz, $CDCl_3$): δ 8.13 (AA'BB', 4H, HAr), 7.80 (s, 4H, HPz), 7.53 (AA'BB', 4H, HAr), 7.20 (AA'BB', 4H, HAr), 6.97 (AA'BB', 4H, HAr), 4.05 (t, $J = 6.8$ Hz, 4H, $-CH_2-O$), 3.56 (s(b), 4H, BH_2), 1.86–1.77 (m, 4H, $-CH_2-CH_2-O$), 1.48–1.28 (m, 28H, $-CH_2-$), 0.89 (t, $J = 6.8$ Hz, 6H, $-CH_3$). ^{13}C NMR (100 MHz, $CDCl_3$): δ 164.7 (C=O), 163.7, 151.1 (Car-O), 137.4 (Cpz-H), 132.6, 132.3, 122.0 (Car-H), 121.2, 120.3 (Car-C), 114.4 (Car-H), 103.7 (Cpz-C), 90.2, 78.7 (C≡C), 68.4 ($-CH_2-O$), 31.9, 29.6, 29.4, 29.3, 29.1, 26.0, 22.7 ($-CH_2-$), 14.1 ($-CH_3$). IR (KBr): 3133 (Csp^2-H), 2461, 2417 (B−H), 2225 (C≡C), 1730 (C=O), 1257 (C−O) cm^{-1}. MS (FAB+) *m/z:* 912 (M^+). Elem Anal. calcd for $C_{56}H_{66}B_2N_4O_6$ (%): C, 73.69; H, 7.29; N, 6.14. Found: C, 73.59; H, 7.22; N, 6.14.

(37) Dingemans, T.; Samulski, E. T. *Liq. Cryst.* **2000**, *27*, 131–136.

(38) Gimeno, M.; Ros, M. B.; Serrano, J. L.; de la Fuente, M. R. *Angew. Chem., Int. Ed.* **2004**, *43*, 5235–5238.

BHC12 *2,6-bis(4″-Dodecyloxybenzoyloxyphenyl-1′-yl-ethynyl)-pyrazabole.* Eluent: 1:1 dichloromethane/hexane. Recrystallization: acetone. ^{1}H NMR (400 MHz, $CDCl_3$): δ 8.13 (AA′BB′, 4H, HAr), 7.80 (s, 4H, HPz), 7.53 (AA′BB′,4H, HAr), 7.21 (AA′BB′, 4H, HAr), 6.97 (AA′BB′, 4H, HAr), 4.04 (t, J = 6.4 Hz, 4H, CH_2−O), 3.59 (s(b), 4H, BH_2), 1.86–1.79 (m, 4H, −CH_2−CH_2−O), 1.51–1.27 (m, 36H, −CH_2−), 0.89 (t, J = 6.4 Hz, 6H, −CH_3). ^{13}C NMR (100 MHz, $CDCl_3$): δ 164.6 (C=O), 163.7, 151.1 (Car−O), 137.4 (Cpz−H), 132.6, 132.3, 122.0 (Car−H), 121.2, 120.3 (Car−C), 114.4 (Car−H), 103.7 (Cpz−C), 90.2, 78.7 (C≡C), 68.4 (−CH_2−O), 31.9, 29.7, 29.6, 29.57, 29.4, 29.1, 26.0, 22.7 (−CH_2−), 14.1 (−CH_3). IR (KBr): 3133 (Csp^2−H), 2461, 2417 (B−H), 2226 (C≡C), 1731 (C=O), 1257 (C−O) cm^{-1}. MS (MALDI+) *m/z:* 967 (M − H). Elem Anal. calcd for $C_{60}H_{74}B_2N_4O_6$ (%): C, 74.38; H, 7.70; N, 5.78. Found: C, 74.74; H, 7.63; N, 5.98.

BHC14 *2,6-bis(4″-Tetradecyloxybenzoyloxyphenyl-1′-yl-ethynyl)pyrazabole.* Eluent: 1:1 dichloromethane/hexane. Recrystallization: acetone. ^{1}H NMR (400 MHz, $CDCl_3$): δ 8.11 (AA′BB′, 4H, HAr), 7.80 (s, 4H, HPz), 7.51 (AA′BB′,4H, HAr), 7.17 (AA′BB′, 4H, HAr), 6.95 (AA′BB′, 4H, HAr), 4.02 (t, J = 6.8 Hz, 4H, −CH_2−O), 3.57 (s(b), 4H, BH_2), 1.86–1.77 (m, 4H, −CH_2−CH_2−O), 1.48–1.28 (m, 44H, −CH_2−), 0.89 (t, J = 6.8 Hz, 6H, −CH_3). ^{13}C NMR (100 MHz, $CDCl_3$): δ 164.6 (C=O), 163.7, 151.1 (Car−O), 137.5 (Cpz−H), 132.6, 132.3, 122.1 (Car−H), 121.2, 120.2 (Car−C), 114.4 (Car−H), 103.7 (Cpz−C), 90.2, 78.6 (C′C), 68.4 (−CH_2−O), 31.9, 29.7, 29.6, 29.4, 29.3, 29.1, 25.9, 22.7 (−CH_2−), 14.1 (−CH_3). IR (KBr): 3138, 3128 (Csp^2−H), 2461, 2414 (B−H), 2230 (C≡C), 1737, 1729 (C=O), 1257 (C−O) cm^{-1}. MS (FAB+) *m/z:* 1023 (M^+). Elem Anal. calcd for $C_{64}H_{82}B_2N_4O_6$ (%): C, 75.00; H, 8.06; N, 5.47. Found: C, 75.12; H, 8.15; N, 5.41.

BHC16 *2,6-bis(4″-Hexadecyloxybenzoyloxyphenyl-1′-yl-ethynyl)pyrazabole.* Eluent: 1:1 dichloromethane/hexane. Recrystallization: acetone. ^{1}H NMR (400 MHz, $CDCl_3$): δ 8.13 (AA′BB′, 4H, HAr), 7.80 (s, 4H, HPz), 7.53 (AA′BB′,4H, HAr), 7.20 (AA′BB′, 4H, HAr), 6.97 (AA′BB′, 4H, HAr), 4.04 (t, J = 6.8 Hz, 4H, −CH_2−O), 3.58 (s(b), 4H, BH_2), 1.86–1.79 (m, 4H, −CH_2−CH_2−O), 1.51–1.26 (m, 52H, −CH_2−), 0.88 (t, J = 6.8 Hz, 6H, −CH_3). ^{13}C NMR (100 MHz, $CDCl_3$): δ 164.7 (C=O), 163.8, 151.1 (Car−O), 137.4 (Cpz−H), 132.6, 132.3, 122.0 (Car−H), 121.2, 120.3 (Car−C), 114.4 (Car−H), 103.8 (Cpz−C), 90.2, 78.7 (C≡C), 68.4 (−CH_2−O), 31.9, 29.7, 29.6, 29.5, 29.3, 29.1, 26.0, 22.7 (−CH_2−), 14.1 (−CH_3). IR (KBr) 3133 (Csp^2−H), 2461, 2417 (B−H), 2225 (C≡C), 1730 (C=O), 1257 (C−O) cm^{-1}. MS (FAB+) *m/z:* 1080 (M^+). Elem Anal. calcd for $C_{68}H_{90}B_2N_4O_6$ (%): C, 75.55; H, 8.39; N, 5.18. Found: C, 75.71; H 8.23; N, 5.38.

BHC18 *2,6-bis(4″-Octadecyloxybenzoyloxyphenyl-1′-yl-ethynyl)pyrazabole.* Eluent: 1:1 dichloromethane/hexane. Recrystallization: acetone. ^{1}H NMR (400 MHz, $CDCl_3$): δ 8.13 (AA′BB′, 4H, HAr), 7.80 (s, 4H, HPz), 7.53 (AA′BB′,4H, HAr), 7.20 (AA′BB′, 4H, HAr), 6.97 (AA′BB′, 4H, HAr), 4.05 (t, J = 6.4 Hz, 4H, −CH_2−O), 3.59 (s(b), 4H, BH_2), 1.86–1.79 (m, 4H, −CH_2−CH_2−O), 1.49–1.26 (m, 60H, −CH_2−), 0.88 (t, J = 6.4 Hz, 6H, −CH_3). ^{13}C NMR (100 MHz, $CDCl_3$): δ 164.7 (C=O), 163.7, 151.1 (Car−O), 137.4 (Cpz−H), 132.6, 132.3, 122.0 (Car−H), 121.2, 120.2 (Car−C), 114.4 (Car−H), 103.7 (Cpz−C), 90.2, 78.6 (C≡C), 68.3 (−CH_2−O), 31.9, 29.7, 29.6, 29.5, 29.4, 29.3, 29.1, 26.0, 22.7 (−CH_2-), 14.1 (−CH_3). IR (KBr) 3133 (Csp^2-H), 2461, 2417 (B-H), 2225 (C≡C), 1730 (C=O), 1257 (C−O) cm^{-1}. MS (FAB+) *m/z:* 1137 (M^+). Elem Anal. calcd for $C_{72}H_{98}B_2N_4O_6$ (%): C, 76.04; H, 8.69; N, 4.93. Found: C, 76.46; H, 8.48; N, 4.85.

BHArC14 *2,6-bis(4′-(4″-Tetradecyloxybenzoyloxy)benzoyloxyphenyl-1′-yl-ethynyl)pyrazabole.* Eluent: 95:5 dichloromethane/hexane. Recrystallization: dichloromethane. ^{1}H NMR (400 MHz, $CDCl_3$): δ 8.27 (AA′BB′, 4H, HAr), 8.15 (AA′BB′, 4H, HAr), 7.81 (s, 4H, HPz), 7.55 (AA′BB′,4H, HAr), 7.38 (AA′BB′, 4H, HAr), 7.23 (AA′BB′, 4H, HAr), 6.99 (AA′BB′, 4H, HAr), 4.02 (t, J = 6.4 Hz, 4H, −CH_2−O), 3.58 (s(b), 4H, BH_2), 1.86–1.78 (m, 4H, −CH_2−CH_2−O), 1.52–1.26 (m, 44H, −CH_2−), 0.88 (t, J = 6.4 Hz, 6H, −CH_3). ^{13}C NMR (100 MHz, $CDCl_3$): δ 164.3, 164.1 (C=O), 163.4, 155.5, 150.8 (Car−O), 137.7 (Cpz−H), 132.7, 132.4, 131.8 (Car−H), 126.5 (Car−C), 122.1, 121.9 (Car−H), 121.4, 120.5 (Car−C), 114.4 (Car−H), 103.5 (Cpz−C), 90.0, 78.9 (C′C), 68.4 (−CH_2−O), 31.9, 29.6, 29.56, 29.5, 29.3, 26.0, 22.7 (−CH_2−), 14.1 (−CH_3). IR (KBr): 3138 (Csp^2−H), 2461, 2417 (B−H), 2227 (C≡C), 1735 (C=O), 1253 (C−O) cm^{-1}. MS (MALDI+) *m/z:* 1263 (M − H). Elem Anal. calcd for $C_{78}H_{90}B_2N_4O_6$ (%): C, 74.05; H, 7.17; N, 4.43. Found: C, 74.21; H, 7.09; N, 4.52.

BHArCox *2,6-bis(4″-(4‴-(2⁗-(2⁗′-(2⁗′-(2⁗′-Methoxyethoxy)-ethoxy)ethoxy)ethoxy) benzoyloxy)benzoyloxyphenyl-1′-yl-ethynyl)pyrazabole.* Eluent: 1:1 dichloromethane/ethyl acetate. Recrystallization: dichloromethane/hexane. ^{1}H NMR (400 MHz, $CDCl_3$): δ 8.28 (AA′BB′, 4H, HAr), 8.16 (AA′BB′, 4H, HAr), 7.81 (s, 4H, HPz), 7.55 (AA′BB′,4H, HAr), 7.38 (AA′BB′, 4H, HAr), 7.23 (AA′BB′, 4H, HAr), 7.02 (AA′BB′, 4H, HAr), 4.23 (m, 4H, −CH_2−O−Ar), 3.91 (m, 4H, −CH_2−CH_2−O−Ar), 3.75 (m, 4H, −CH_2−), 3.71–3.64 (m, 16H, −CH_2−CH_2−O−CH_3), 3.55 (m, 4H, −CH_2−CH_2−O−CH_3), 3.38 (s, 6H, −CH_3). ^{13}C NMR (100 MHz, $CDCl_3$): δ 164.2, 164.1 (C=O), 163.4, 155.4, 150.8 (Car−O), 137.4 (Cpz−H), 132.7, 132.4, 131.8 (Car−H), 126.6 (Car−C), 122.1, 121.9 (Car−H), 121.3, 120.5 (Car−C), 114.5 (Car−H), 103.6 (Cpz−C), 90.1, 78.8 (C≡C), 71.9, 70.9, 70.6–70.5, 69.5, 67.7 (−CH_2−O), 59.0 (−CH_3−O). IR (KBr) 3135 (Csp^2−H), 2458, 2414 (B−H), 2227 (C≡C), 1734 (C=O), 1266 (C−O) cm^{-1}. MS (MALDI+) *m/z*: 1251 (M − H). Elem Anal. calcd for $C_{68}H_{70}B_2N_4O_6$ (%): C, 65.19; H, 5.63; N, 4.47. Found: C, 64.89; H, 5.70; N, 4.52.

Acknowledgment. This work was supported by the MEC (Spain)−FEDER (EU) funds under the projects MAT2003-07806-C01 and MAT2006-13571-CO2-01, the Ramón y Cajal program (R.G.), the FPU program (E.C.), and the Gobierno de Aragón.

CM702129S